62 (2017) APPLICATIONS OF MATHEMATICS No. 6, 633–659

TIME-DEPENDENT NUMERICAL MODELING OF LARGE-SCALE ASTROPHYSICAL PROCESSES: FROM RELATIVELY SMOOTH FLOWS TO EXPLOSIVE EVENTS WITH EXTREMELY LARGE DISCONTINUITIES AND HIGH MACH NUMBERS

Petr Kurfürst, Jiří Krtička, Brno

Received May 25, 2017. First published November 23, 2017.

Abstract. We calculate self-consistent time-dependent models of astrophysical processes. We have developed two types of our own (magneto) hydrodynamic codes, either the operator-split, finite volume Eulerian code on a staggered grid for smooth hydrodynamic flows, or the finite volume unsplit code based on the Roe's method for explosive events with extremely large discontinuities and highly supersonic outbursts. Both the types of the codes use the second order Navier-Stokes viscosity to realistically model the viscous and dissipative effects. They are transformed to all basic orthogonal curvilinear coordinate systems as well as to a special non-orthogonal geometric system that fits to modeling of astrophysical disks. We describe mathematical background of our codes and their implementation for astrophysical simulations, including choice of initial and boundary conditions. We demonstrate some calculated models and compare the practical usage of numerically different types of codes.

Keywords: Eulerian hydrodynamics; finite volume; operator-split method; unsplit method; Roe's method; curvilinear coordinates

MSC 2010: 76N15, 85-08

1. Introduction

Attempting to realistically model astrophysical processes leads to extreme physical and geometric situations, and hence to extreme demands on the mathematical efficiency and accuracy of computational algorithms. One of the major problems is

The access to computing and storage facilities owned by parties and projects contributing to the National Grid Infrastructure MetaCentrum, provided under the program "Projects of Large Infrastructure for Research, Development, and Innovations" (LM2010005) is appreciated. The research has been supported by the grant GA ČR GA16-01116S.

the vast dimension of modeled systems that however cannot simply be re-scaled due to the necessity to include an ultimate propagation speed of pressure perturbations (related to the sound speed in a given medium). Another common problem is the extreme disproportionality either in geometry or in physical characteristics. For example, in case of various types of circumstellar disks (see Section 2.1) we have to extend the radial computational domain up to several hundreds of stellar radii (the order of 10^{10} km), while the vertical scale-height of the disk in the region very close to the star is approximately 5 orders of magnitude smaller. This region is however crucial for feeding the disk with mass and angular momentum, therefore it cannot be excluded or marginalized off the computation. In thermonuclear supernovae (type Ia) the size of the problem is of the order 10^3 km while the thickness of the physically most important region, the combustion (detonation) wave where most of thermonuclear reactions occur, is of the order of 10^{-3} m. To model the interactions of expanding envelopes of supernovae, we have to deal with an extreme jump in velocity and pressure that reaches up to several tens of orders of magnitude within quite narrow discontinuity (shock wave). Moreover, we can solve almost none of the problems in Cartesian geometry, and we usually have to employ the spherical coordinates (for stars, expanding envelopes, and stellar winds), the cylindrical coordinates (in the case of rotational symmetry and circumstellar disks) or even more specific coordinate systems (see Section 3).

To overcome these difficulties, one has developed various tools that are widely used in (not only) astrophysical community. Regarding the methods of numerical grids, moving meshes, static or adaptive mesh refinement, or methods of artificial broadening of very thin or small however physically crucially important regions are employed. Various numerical principles of the computational codes also fit to computation of various physical kinds of problems. Within the purpose of our hydrodynamic calculations we basically distinguish two such computational kinds. Either the relatively smooth flow of gas, i.e., where the sharp or even discontinuous jumps in pressure do not exceed 2–3 orders of magnitude, or discontinuous flows where these jumps may be much higher. The latter is principally associated with highly supersonic flows where for example in an expanding envelope of supernova the values of Mach number may reach 10^2–10^3.

We demonstrate two different astrophysical problems: the relatively smooth hydrodynamic solution of circumstellar outflowing disks and the extremely discontinuous interaction of the expanding envelope of supernova with an asymmetrical circumstellar environment. We have developed and used two classes of hydrodynamic codes that are based on the following methods: 1) the operator-split (ZEUS-like) time-dependent finite volume Eulerian scheme on staggered grid for (relatively) smooth hydrodynamic calculations [9], [11], [12], [13], [28] of circumstellar disks, and 2) our

own version of the single-step (unsplit, ATHENA-like) time-dependent finite volume Eulerian hydrodynamic algorithm based on the Roe's method [23], [27], [29] for highly discontinuous flows in expanding envelopes of supernovae [13] (we have programmed all the codes in FORTRAN 95). We model the circumstellar outflowing disks in a special coordinate system ("flaring geometry", see Section 3), using however alternatively both the types of hydrodynamic codes. We can successfully calculate the interaction of supernova envelope with circumstellar environment in the Cartesian grid using merely the second code type.

We have properly tested our codes within the test problems (Riemann-Sod shock tube, Kelvin-Helmholtz instability) and used them for calculations of the 1D and 2D circumstellar disk structure and for the study of interactions of expanding envelopes of supernovae with asymmetrically distributed circumstellar environment. In the paper we describe the main numerical principles of both types of the hydrodynamic codes (see Sections 4.1 and 4.2). We also demonstrate the results on selected astrophysical simulations and compare the convenience of the codes and of the corresponding numerical principles in Sections 5.1 and 5.2.

2. Basics of analytical solution of simulated astrophysical processes

In this section we provide the basic description of solved astrophysical problems. In Section 2.1 we introduce the basic hydrodynamic equations in the explicit form used in our calculations. We do not involve magnetohydrodynamic terms, since they are not employed in the calculations referred in this paper. In the following Sections 2.2 and 2.3 we describe the basic physical background of simulated astrophysical problems.

2.1. Explicit form of hydrodynamic equations. The following nonlinear system of equations represents the fundamental conservation laws of mass, momentum and energy, forming thus the base of the hydrodynamic calculations. We strictly keep hereinafter the following notation: the capital letters R and V denote radial distance and velocity in cylindrical and in special non-orthogonal "flaring disk" coordinate systems introduced in Section 3 (where R and V denote the norms of the vectors while the vectors themselves are denoted in general using bold capitals), while we use the small letters r and v for the same quantities in Cartesian and in spherical coordinate systems.

Continuity equation (mass conservation law) in the general form is

$$\frac{\partial \varrho}{\partial t} + \boldsymbol{\nabla} \cdot (\varrho \boldsymbol{V}) = 0, \tag{2.1}$$

where ϱ is the mass density, t is the time, $\boldsymbol{V}$ is the vector of velocity, and the operator of divergence takes the particular form according to the coordinate system used. Equation of motion (conservation of momentum or angular momentum) generally is

$$\frac{\partial(\varrho\boldsymbol{V})}{\partial t} + \boldsymbol{\nabla}\cdot(\varrho\boldsymbol{V}\otimes\boldsymbol{V}) = -\boldsymbol{\nabla}P - \varrho\boldsymbol{\nabla}\Phi + \boldsymbol{f}_{\mathrm{visc}} + \boldsymbol{f}_{\mathrm{rad}}, \tag{2.2}$$

where P is the scalar pressure, Φ is the gravitational potential, $\boldsymbol{f}_{\mathrm{visc}}$ and $\boldsymbol{f}_{\mathrm{rad}}$ are the contributions of viscous and radiative force densities. The energy equation in the full form (where E is the total energy)

$$\frac{\partial E}{\partial t} + \boldsymbol{\nabla}\cdot(E\boldsymbol{V}) = -\boldsymbol{\nabla}\cdot(\mathcal{P}\boldsymbol{V} + \boldsymbol{q}) + \boldsymbol{f}\cdot\boldsymbol{V}, \quad E = \varrho\varepsilon + \frac{\varrho V^2}{2}, \tag{2.3}$$

is involved only in processes, where the kinetic or heat energy is dominantly generated within the system itself (we usually regard such systems as adiabatic). In equation (2.3), $\mathcal{P}$ denotes the complete pressure tensor (including non-diagonal viscosity), $\boldsymbol{q}$ is the vector of the flux of thermal energy (heating or cooling), $\boldsymbol{f}$ is the sum of all external force densities, and ε is the specific internal (heat) energy. The set of hydrodynamic equations is closed by the equation of state, whose explicit adiabatic or isothermal form, respectively, is

$$P = (\gamma-1)\Big(E - \frac{\varrho V^2}{2}\Big), \quad P = \varrho a^2, \tag{2.4}$$

where γ denotes the adiabatic index (ratio of specific heats) and a is the isothermal speed of sound.

2.2. Determining equations of viscous and heat effects in circumstellar disks. The axisymmetric kinematics of the disks requires intrinsically cylindrical or even the special "flaring disk" geometry (see Section 3, see also [11]). In order to express equation (2.1) in terms of constant mass-loss rate $\dot{M}$ of a stationary system, we introduce the (vertically) integrated column (surface) density $\Sigma = \int_{-\infty}^{\infty}\varrho\,\mathrm{d}z$. The cylindrical form of equation (2.1) thus becomes $\dot{M} = 2\pi R\Sigma V_R$, where V_R is the radial velocity component of the gas flow. We introduce also the disk vertical scale-height H defined as $H = a/\Omega$, where $\Omega = V_\varphi/R$ is the angular velocity, while V_φ is the azimuthal ("rotational") velocity component of the gas flow (considered approximately as Keplerian, i.e., $V_\varphi^2 = GM_\star/R$, where G is the gravitational constant and $M_\star$ is the mass of the central star). In case of constant temperature T (with $a \sim \sqrt{T} = \text{const.}$), the vertical flaring angle of the disk grows with distance as $H \propto R^{3/2}$ (see Fig. 1). Assuming the vertical hydrostatic equilibrium $\mathrm{d}P/\mathrm{d}z = -\varrho g_z$ in the stationary disk structure (where g_z is the vertical component of gravitational

acceleration), we obtain by its integration the approximate vertical density profile of the thin circumstellar disk [10], [14],

$$\varrho \approx \varrho_{\mathrm{eq}} \exp\Big(-\frac{z^2}{2H^2}\Big), \quad \varrho_{\mathrm{eq}} = \frac{\Sigma}{\sqrt{2\pi}H}, \tag{2.5}$$

where we obtain the latter relation for the density ϱ_{eq} in the disk equatorial plane (midplane) by integrating the equation of the surface density Σ. Conservation of angular momentum $\mathrm{d}\boldsymbol{J}/\mathrm{d}t = \boldsymbol{G}$, where the torque $\boldsymbol{G}$ is produced by the $R\varphi$ component $G_{R\varphi,\mathrm{visc}}$ of the viscous stress tensor, gives the explicit azimuthal momentum component equation (see also [11], [12])

$$\frac{\partial}{\partial t}(R\varrho V_\varphi) + \frac{1}{R}\frac{\partial}{\partial R}\Big(R^2\varrho V_R V_\varphi - \alpha a^2 R^3 \varrho \frac{\partial \ln V_\varphi}{\partial R} + \alpha a^2 R^2 \varrho\Big) = 0, \tag{2.6}$$

where the last two terms represent the viscous torque $G_{R\varphi,\mathrm{visc}}$. Inclusion of both the viscosity terms means the second order Navier-Stokes viscosity, while inclusion of only the last term describes the first order Navier-Stokes viscosity [12]. The first order Navier-Stokes viscosity is most frequently used in literature. The second order term increases the efficiency of viscosity in case of Keplerian azimuthal velocity up to the factor 3/2, it also prevents the physically implausible transition to a backward (negative) azimuthal motion of some disk regions in calculations. The α parameter of viscosity [25] is defined as the ratio of the assumed turbulent velocity and the sound speed, $\alpha = V_{\mathrm{turb}}/a \sim \nu/(\lambda a)$, where ν is the standard kinematic viscosity and λ is the mean free path of turbulent eddies (or fluid parcels) of the gas. We examine in our models the radial variations $\alpha \sim \alpha_0 R^{-n}$ with a free parameter $0 < n < 0.2$, where $0.01 < \alpha_0 < 1$ is the disk base viscosity (near the stellar surface).

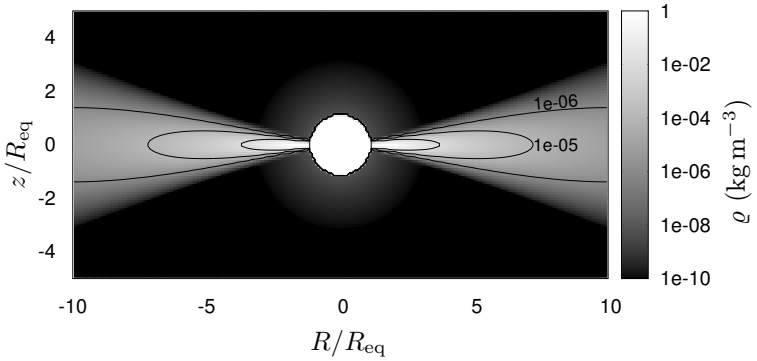

Figure 1. Stationary model of the circumstellar viscous disk density profile, highlighted by the contour lines (marked by the corresponding density). The "flaring" shape of the disk in the vertical sense is demonstrated. We denote by R_{eq} the stellar equatorial radius which may in case of rapidly rotating stars differ from the stellar polar radius up to the factor 3/2 (cf. Fig. 2).

The temperature structure of the disk material is dominantly affected by the irradiation flux from the central star, therefore we regard it as isothermal (which means that the system is in a radiative equilibrium, maintained primarily by an external source of energy). The heat generated by the viscosity also plays a role in the cores of very dense disks, but except extremely massive disks this contribution is only minor. The detail description of the energy physics is very complicated exceeding thus the scope of this paper. It has to take into account all the effects of rotational distortion of the central star, density ϱ, opacity, and chemical composition of the irradiated disk gas and the effects of radiative cooling in the optically thin layers. We calculate numerically all these effects using special programs or subroutines that are involved in the main hydrodynamic code. We introduce here only the fundamental equation of the local temperature gradient (assuming radiative and thermal equilibrium) [17], [18], [19] along a "line-of-sight" direction $\boldsymbol{n}$,

$$\frac{\mathrm{d}T(R,z)}{\mathrm{d}\boldsymbol{n}} = \frac{3\mathcal{F}(R,z)}{16\sigma T^3(R,z)} \frac{\mathrm{d}\tau(R,z)}{\mathrm{d}\boldsymbol{n}}, \tag{2.7}$$

where $\mathcal{F}$ is the local sum of (frequency integrated) irradiative and viscous heat flux (reduced by radiative cooling) and σ is the Stefan-Boltzmann constant. The gradient of the optical depth τ along the same "line-of-sight" direction $\boldsymbol{n}$ is $\mathrm{d}\tau/\mathrm{d}\boldsymbol{n} = -\kappa\varrho\,\hat{\boldsymbol{n}}$, where κ is the opacity of the material with assumed chemical composition, and $\hat{\boldsymbol{n}}$ is the unit vector in the direction $\boldsymbol{n}$.

2.3. Hydrodynamics and similarity conditions in expanding supernova envelope. The basic analytical solution of the supernova (SN) explosive event follows the idea of homologous ($v \propto r/t$) energy-conserving hydrodynamic expansion, using the Sedov-Taylor blast wave solution with different density profiles of an internal gas and surrounding medium [24], [33]. Gravitational force is quite unimportant except for the very interior layers. The radiative losses are almost negligible in the early phase of expansion comparing to the kinetic energy of the gas, we thus regard the process as adiabatic. The scaling parameters are the energy of explosion E_{SN}, mass M_{ej} of the expanding ejecta, and initial stellar radius $R_\star$. Since the main aim of our study is the interaction between the expanding SN-remnant sphere and the surrounding circumstellar media, which may be spherically symmetric (stellar winds, pre-explosion gaseous shells) or asymmetric (circumstellar disks, disk-like density enhancements, bipolar lobes), we neglect a pre-explosion SN interior density distribution, which is completely transformed during the explosion and, on the other hand, is of little influence on the structure of the studied interaction.

During the expansion of a highly supersonic ejecta into the surrounding medium a strong shock wave is driven ahead at the radius $R(t)$. The high pressure behind

the forward shock drives a reverse shock backward into the ejecta, while the relative velocity of this reverse shock is much lower than the velocity of the ejecta themselves [4], [5], [30]. Contact discontinuity separates the SN-remnant and circumstellar media and propagates between the two shock waves. In the reference frame that is co-moving with the forward shock, omitting viscosity and assuming constant adiabatic exponent γ (which is astrophysically relevant), we can rewrite the (spherical) adiabatic hydrodynamic equations (2.1), (2.2), and (2.3) on both sides of the shock front into the simple conservative form [33],

$$\varrho_1 v_1 = \varrho_0 v_0, \quad \varrho_1 v_1^2 + P_1 = \varrho_0 v_0^2 + P_0, \quad \frac{\gamma}{\gamma-1}\frac{P_1}{\varrho_1} + \frac{v_1^2}{2} = \frac{\gamma}{\gamma-1}\frac{P_0}{\varrho_0} + \frac{v_0^2}{2}, \tag{2.8}$$

where the upstream and downstream quantities are respectively labeled with subscripts 0 and 1. The same velocities in the laboratory frame are $D - v_0$ and $D - v_1$, where we denote by D the propagation speed of the forward shock. In the early phase after explosion we approximate the process as a free expansion with the internal velocity v of the gas proportional to the radius r. Assuming the density profile $\varrho_{\rm in}$ in the envelope as a (time-dependent) power law and the density of the surrounding (static) medium $\varrho_{\rm out}$ as an alternate power-law, we obtain the fundamental relations

$$v = \frac{r}{t}, \quad \varrho_{\rm in}(t) = Ar^{-n}t^{n-3}, \quad \varrho_{\rm out} = Br^{-\omega}, \tag{2.9}$$

where A, B, n, ω are particular constants. Equation (2.9) gives the corresponding pressure relations $P_{\rm in}(t) = \widetilde{A}r^{2-n}t^{n-5}$ and $P_{\rm out} = \widetilde{B}\varrho_{\rm out}^{\gamma}$, $P_{\rm out} \ll P_{\rm in}$, where $\widetilde{A}$ and $\widetilde{B}$ are different constants, $P_{\rm out}$ is the pressure in the surrounding medium, and $P_{\rm in}$ is the pressure in the expanding SN envelope. The subsequent analytical approach requires a formalism of a similarity solution (see, e.g., [4], [20], [24], [33]) which leads to the constraints $\omega < 3$ and $n > 5$. The basic solution is also described in [13].

3. Flaring disk coordinates

3.1. Equations of coordinate transformation, differential operators. We have developed the unique coordinate system that basically fits the geometry of circumstellar disks, adapting vertical hydrostatic equilibrium as well as the opening angle of the "flaring disk" geometry [11], [13]. The radial R and azimuthal φ coordinates are identical with standard the cylindrical coordinate system, and the coordinate θ is defined as the elevation angle calculated in positive and negative direction from the equatorial plane. However, the real shape of the disks limits the elevation angle to $\theta \in \langle -\pi/4, \pi/4\rangle$ in a maximum case, therefore we do not specify the boundary condition $\theta = \pi/2$. Figure 2 illustrates the system in the R-θ plane.

Transformation equations and the transformation of the unit basis vectors (denoted using the "hat" symbol) are

$$x = R\cos\varphi, \quad y = R\sin\varphi, \quad z = R\tan\theta, \tag{3.1}$$

$$\hat{\boldsymbol{x}} = \hat{\boldsymbol{R}}\cos\varphi - \hat{\boldsymbol{\varphi}}\sin\varphi, \quad \hat{\boldsymbol{y}} = \hat{\boldsymbol{R}}\sin\varphi + \hat{\boldsymbol{\varphi}}\cos\varphi, \quad \hat{\boldsymbol{z}} = \frac{\hat{\boldsymbol{R}}\sin\theta + \hat{\boldsymbol{\theta}}}{\cos\theta}, \tag{3.2}$$

where the expressions for the unit vectors $\hat{\boldsymbol{x}}$ and $\hat{\boldsymbol{y}}$ are identical with the standard cylindrical coordinate system. The derivation of the transformation equation for the vector $\hat{\boldsymbol{z}}$ is illustrated in Fig. 3. The configuration of the unit basis vectors shows that the transformation equation $\hat{\boldsymbol{\theta}} = -\hat{\boldsymbol{R}}\sin\theta + \hat{\boldsymbol{z}}\cos\theta$ holds for the lower and upper half-space with either negative or positive z and θ coordinates.

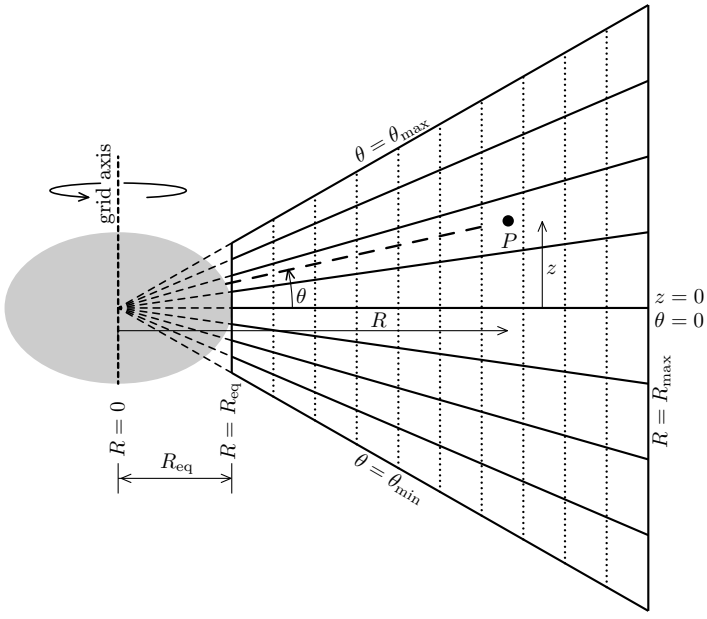

Figure 2. Schematic chart of the flaring disk coordinate system in R-θ plane. Intersection of the coordinate surface S_θ containing a point P with the R-θ plane is highlighted by the thick dashed line. The parameters $R_{\rm eq}$, $R_{\max}$, and $\theta_{\min}$ (or $\theta_{\max}$) are entered into the code. The rotationally oblate central star is depicted by a light gray ellipse.

Angular and time derivatives of the unit basis vectors $\hat{\boldsymbol{R}}$ and $\hat{\boldsymbol{\varphi}}$ are the same as in standard cylindrical system, angular and time derivatives of the unit basis vector $\hat{\boldsymbol{\theta}}$ are

$$\frac{\partial\hat{\boldsymbol{\theta}}}{\partial\varphi} = -\hat{\boldsymbol{\varphi}}\sin\theta, \quad \frac{\partial\hat{\boldsymbol{\theta}}}{\partial\theta} = -\frac{\hat{\boldsymbol{R}} + \hat{\boldsymbol{\theta}}\sin\theta}{\cos\theta}, \quad \frac{\partial\hat{\boldsymbol{\theta}}}{\partial t} = -\frac{\hat{\boldsymbol{R}}\dot{\theta}}{\cos\theta} - \hat{\boldsymbol{\varphi}}\dot{\varphi}\sin\theta - \hat{\boldsymbol{\theta}}\dot{\theta}\tan\theta, \tag{3.3}$$

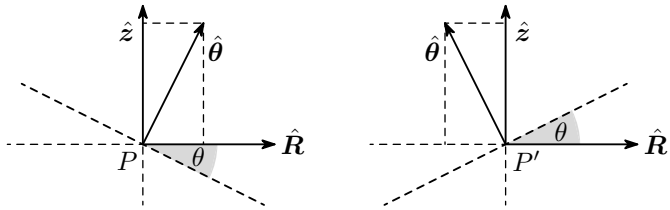

Figure 3. *Left panel*: Configuration of radial and "vertical" unit basis vectors of the standard cylindrical and the flaring coordinate system at an arbitrary point P in the "lower" half-space of the disk, i.e., with negative z and θ coordinates. The unit basis vector $\hat{\boldsymbol{R}}$ is identical for both the systems while the vectors $\hat{\boldsymbol{z}}$ and $\hat{\boldsymbol{\theta}}$ form the bases of the standard cylindrical and the flaring coordinate system, respectively. The thick dashed line denotes the coordinate surface S_θ (where the coordinate θ is constant). *Right panel*: As in the left panel, at an arbitrary point P' in the "upper" half-space of the disk, i.e., with positive coordinates z and θ. Other principles and the notation are the same as in Fig. 2.

the transformation Jacobian is $J = R^2/\cos^2\theta$. Metric tensors g (in variables R, φ, θ) are

$$(g_{ij}) = \begin{pmatrix} \dfrac{1}{\cos^2\theta} & 0 & \dfrac{R\sin\theta}{\cos^3\theta} \\ 0 & R^2 & 0 \\ \dfrac{R\sin\theta}{\cos^3\theta} & 0 & \dfrac{R^2}{\cos^4\theta} \end{pmatrix}, \quad (g^{ij}) = \begin{pmatrix} 1 & 0 & -\dfrac{\sin 2\theta}{2R} \\ 0 & \dfrac{1}{R^2} & 0 \\ -\dfrac{\sin 2\theta}{2R} & 0 & \dfrac{\cos^2\theta}{R^2} \end{pmatrix}. \tag{3.4}$$

The volume bounded by the coordinate surfaces (with constant R_2, R_1, φ_1, φ_2, θ_1, θ_2) is

$$V = \frac{R_2^3 - R_1^3}{3}(\varphi_2 - \varphi_1)(|\tan\theta_2| - |\tan\theta_1|). \tag{3.5}$$

The areas of the corresponding grid cell surfaces (the subscripts refer to the coordinate that is constant on a given surface) are

$$\begin{aligned} S_R &= R^2(\varphi_2 - \varphi_1)(|\tan\theta_2| - |\tan\theta_1|), \\ S_\varphi &= \frac{R_2^2 - R_1^2}{2}(|\tan\theta_2| - |\tan\theta_1|), \\ S_\theta &= \frac{R_2^2 - R_1^2}{2}\frac{(\varphi_2 - \varphi_1)}{\cos\theta}. \end{aligned} \tag{3.6}$$

The gradient of a scalar function $f = f(R, \varphi, \theta)$ is

$$\boldsymbol{\nabla} f = \hat{\boldsymbol{R}}\frac{\partial f}{\partial R} + \hat{\boldsymbol{\varphi}}\frac{1}{R}\frac{\partial f}{\partial \varphi} + \hat{\boldsymbol{\theta}}\frac{\cos\theta}{R}\frac{\partial f}{\partial \theta}. \tag{3.7}$$

The gradient of an arbitrary vector field $\boldsymbol{A}(R,\varphi,\theta)$ is the matrix $\boldsymbol{\nabla A}$ with elements

$$(3.8)\qquad (\boldsymbol{\nabla A})_{11}=\frac{\partial A_R}{\partial R}\hat{\boldsymbol{R}}\hat{\boldsymbol{R}},\quad (\boldsymbol{\nabla A})_{12}=\frac{\partial A_\varphi}{\partial R}\hat{\boldsymbol{R}}\hat{\boldsymbol{\varphi}},\quad (\boldsymbol{\nabla A})_{13}=\frac{\partial A_\theta}{\partial R}\hat{\boldsymbol{R}}\hat{\boldsymbol{\theta}},$$
$$(\boldsymbol{\nabla A})_{21}=\Big(\frac{1}{R}\frac{\partial A_R}{\partial\varphi}-\frac{A_\varphi}{R}\Big)\hat{\boldsymbol{\varphi}}\hat{\boldsymbol{R}},$$
$$(\boldsymbol{\nabla A})_{22}=\Big(\frac{1}{R}\frac{\partial A_\varphi}{\partial\varphi}+\frac{A_R}{R}-\frac{A_\theta\sin\theta}{R}\Big)\hat{\boldsymbol{\varphi}}\hat{\boldsymbol{\varphi}},$$
$$(\boldsymbol{\nabla A})_{23}=\frac{1}{R}\frac{\partial A_\theta}{\partial\varphi}\hat{\boldsymbol{\varphi}}\hat{\boldsymbol{\theta}},\quad (\boldsymbol{\nabla A})_{31}=\Big(\frac{\cos\theta}{R}\frac{\partial A_R}{\partial\theta}-\frac{A_\theta}{R}\Big)\hat{\boldsymbol{\theta}}\hat{\boldsymbol{R}},$$
$$(\boldsymbol{\nabla A})_{32}=\frac{\cos\theta}{R}\frac{\partial A_\varphi}{\partial\theta}\hat{\boldsymbol{\theta}}\hat{\boldsymbol{\varphi}},\quad (\boldsymbol{\nabla A})_{33}=\Big(\frac{\cos\theta}{R}\frac{\partial A_\theta}{\partial\theta}-\frac{A_\theta\sin\theta}{R}\Big)\hat{\boldsymbol{\theta}}\hat{\boldsymbol{\theta}}.$$

The divergence of an arbitrary vector field $\boldsymbol{A}(R,\varphi,\theta)$ (noting that $\hat{\boldsymbol{R}}\cdot\hat{\boldsymbol{\theta}}=-\sin\theta$) is

$$(3.9)\qquad \boldsymbol{\nabla}\cdot\boldsymbol{A}=\frac{1}{R}\frac{\partial(RA_R)}{\partial R}+\frac{1}{R}\frac{\partial A_\varphi}{\partial\varphi}+\frac{\cos\theta}{R}\frac{\partial A_\theta}{\partial\theta}-\frac{\sin\theta}{R}\Big[\frac{\partial(RA_\theta)}{\partial R}+\cos\theta\frac{\partial A_R}{\partial\theta}\Big].$$

The curl of a vector $\boldsymbol{A}(R,\varphi,\theta)$, where the cross products of different basis vectors are

$$(3.10)\qquad \hat{\boldsymbol{R}}\times\hat{\boldsymbol{\varphi}}=\frac{\hat{\boldsymbol{R}}\sin\theta+\hat{\boldsymbol{\theta}}}{\cos\theta},\quad \hat{\boldsymbol{\varphi}}\times\hat{\boldsymbol{\theta}}=\frac{\hat{\boldsymbol{R}}+\hat{\boldsymbol{\theta}}\sin\theta}{\cos\theta},\quad \hat{\boldsymbol{\theta}}\times\hat{\boldsymbol{R}}=\hat{\boldsymbol{\varphi}}\cos\theta,$$

takes the explicit form

$$\begin{aligned}(3.11)\quad \boldsymbol{\nabla}\times\boldsymbol{A}=\hat{\boldsymbol{R}}\Big\{&\frac{\tan\theta}{R}\Big[\frac{\partial(RA_\varphi)}{\partial R}-\frac{\partial A_R}{\partial\varphi}\Big]+\frac{1}{R}\Big(\frac{1}{\cos\theta}\frac{\partial A_\theta}{\partial\varphi}-\frac{\partial A_\varphi}{\partial\theta}\Big)\Big\}\\
&+\hat{\boldsymbol{\varphi}}\Big\{\frac{\cos\theta}{R}\Big[\cos\theta\frac{\partial A_R}{\partial\theta}-\frac{\partial(RA_\theta)}{\partial R}\Big]\Big\}\\
&+\hat{\boldsymbol{\theta}}\Big\{\frac{1}{R\cos\theta}\Big[\frac{\partial}{\partial R}(RA_\varphi)-\frac{\partial A_R}{\partial\varphi}\Big]+\frac{\sin\theta}{R}\Big(\frac{1}{\cos\theta}\frac{\partial A_\theta}{\partial\varphi}-\frac{\partial A_\varphi}{\partial\theta}\Big)\Big\}.\end{aligned}$$

The Laplacian operator in the flaring disk system becomes

$$(3.12)\qquad \Delta=\frac{1}{R}\frac{\partial}{\partial R}\Big(R\frac{\partial}{\partial R}\Big)+\frac{1}{R^2}\frac{\partial^2}{\partial\varphi^2}+\frac{\cos\theta}{R^2}\frac{\partial}{\partial\theta}\Big(\cos\theta\frac{\partial}{\partial\theta}\Big)-\frac{2\sin\theta\cos\theta}{R}\frac{\partial^2}{\partial R\,\partial\theta}.$$

3.2. Velocity and acceleration. The position vector $\boldsymbol{r}$ and the velocity vector $\boldsymbol{V}=\mathrm{d}\boldsymbol{r}/\mathrm{d}t=V_R\hat{\boldsymbol{R}}+V_\varphi\hat{\boldsymbol{\varphi}}+V_\theta\hat{\boldsymbol{\theta}}$ in this coordinate system is

$$(3.13)\qquad \boldsymbol{r}=x\hat{\boldsymbol{x}}+y\hat{\boldsymbol{y}}+z\hat{\boldsymbol{z}}=\frac{\hat{\boldsymbol{R}}R+\hat{\boldsymbol{\theta}}R\sin\theta}{\cos^2\theta},$$

$$(3.14)\qquad \boldsymbol{V}=\hat{\boldsymbol{R}}\Big(\frac{\dot{R}+R\dot{\theta}\,\tan\theta}{\cos^2\theta}\Big)+\hat{\boldsymbol{\varphi}}R\dot{\varphi}+\hat{\boldsymbol{\theta}}\Big(\frac{\dot{R}\tan\theta}{\cos\theta}+\frac{R\dot{\theta}}{\cos^3\theta}\Big).$$

The components of the acceleration vector $\boldsymbol{a} = \mathrm{d}\boldsymbol{V}/\mathrm{d}t = a_R\hat{\boldsymbol{R}} + a_\varphi\hat{\boldsymbol{\varphi}} + a_\theta\hat{\boldsymbol{\theta}}$ are

$$a_R = \frac{\ddot{R} + R\ddot{\theta}\tan\theta + 2\dot{\theta}(\dot{R} + R\dot{\theta}\tan\theta)\tan\theta}{\cos^2\theta} - R\dot{\varphi}^2, \tag{3.15}$$

$$a_\varphi = R\ddot{\varphi} + 2\dot{R}\dot{\varphi}, \quad a_\theta = \frac{1}{\cos\theta}\Big[\ddot{R}\tan\theta + \frac{R\ddot{\theta} + 2\dot{\theta}(\dot{R} + R\dot{\theta}\,\tan\theta)}{\cos^2\theta}\Big].$$

Using equations (3.13) and (3.15), we express the components of the velocity vector as

$$\dot{R} = V_R - V_\theta\sin\theta, \quad \dot{\varphi} = \frac{V_\varphi}{R}, \quad \dot{\theta} = \frac{(V_\theta - V_R\sin\theta)\cos\theta}{R}. \tag{3.16}$$

The components of the vector $\boldsymbol{a}$ in terms of the velocity vector components (noting that $\mathrm{d}\boldsymbol{V}/\mathrm{d}t = \partial\boldsymbol{V}/\partial t + \boldsymbol{V}\cdot\boldsymbol{\nabla}\boldsymbol{V}$) are

$$a_R = \frac{\partial V_R}{\partial t} + \underbrace{V_R\frac{\partial V_R}{\partial R} + \frac{V_\varphi}{R}\frac{\partial V_R}{\partial\varphi} + V_\theta\frac{\cos\theta}{R}\frac{\partial V_R}{\partial\theta}}_{(\vec{V}\cdot\vec{\nabla})V_R} - \frac{V_\varphi^2 + V_\theta^2}{R} + \frac{V_R V_\theta\sin\theta}{R}, \tag{3.17}$$

$$a_\varphi = \frac{\partial V_\varphi}{\partial t} + \underbrace{V_R\frac{\partial V_\varphi}{\partial R} + \frac{V_\varphi}{R}\frac{\partial V_\varphi}{\partial\varphi} + V_\theta\frac{\cos\theta}{R}\frac{\partial V_\varphi}{\partial\theta}}_{(\vec{V}\cdot\vec{\nabla})V_\varphi} + \frac{V_R V_\varphi}{R} - \frac{V_\varphi V_\theta\sin\theta}{R}, \tag{3.18}$$

$$a_\theta = \frac{\partial V_\theta}{\partial t} + \underbrace{V_R\frac{\partial V_\theta}{\partial R} + \frac{V_\varphi}{R}\frac{\partial V_\theta}{\partial\varphi} + V_\theta\frac{\cos\theta}{R}\frac{\partial V_\theta}{\partial\theta}}_{(\vec{V}\cdot\vec{\nabla})V_\theta} - \frac{V_\theta^2\sin\theta}{R} + \frac{V_R V_\theta\sin^2\theta}{R}. \tag{3.19}$$

The underbraced terms on the right-hand sides (RHS) of equations (3.17)–(3.19) express the nonlinear advection while the other terms represent the fictitious forces.

We express the velocity vector components V_R, V_φ, V_θ from equations (3.1) and (3.16) in terms of the cylindrical velocity vector components $V_{R,\mathrm{cyl}}$, $V_{\varphi,\mathrm{cyl}}$, V_z:

$$V_R = V_{R,\mathrm{cyl}} + V_z\tan\theta, \quad V_\varphi = V_{\varphi,\mathrm{cyl}}, \quad V_\theta = \frac{V_z}{\cos\theta}. \tag{3.20}$$

In case of perfect vertical hydrostatic balance, $V_z = 0$, equations (3.17)–(3.19) become identical to standard cylindrical coordinates, which is an essential simplification of the mathematical complexity. The advantage of flaring coordinates, however, lies in the similarity of the grid shape to the described astrophysical system, thus enabling us to efficiently and smoothly calculate the hydrodynamics within the extremely narrow inner part of the disk.

4. Numerical methods

4.1. Operator-split finite volume scheme for smooth hydrodynamics. Equations (2.1)–(2.3) are discretized using time-explicit operator-splitting (see equation (4.2)) and finite volume method on staggered radial grids [6], [15], [16], when the two parallel grids A for vectors and B for scalars are shifted by half of the spatial step in each direction (see also [11]). The advection fluxes are calculated on the boundaries of the grid cells [15], [16], [22] using van Leer monotonic interpolation [31], [32] (equation (4.10)). We write the full equations (2.1)–(2.3) (where we denote the RHS terms as source terms) and their left-hand sides (LHS, usually designated as *advection scheme*), respectively, in compact *conservative* form schematically as [11]

$$\frac{\mathrm{d}\boldsymbol{U}}{\mathrm{d}t}\Big|_{\mathrm{full}} = \mathcal{L}(\boldsymbol{U}), \qquad \frac{\partial \boldsymbol{U}}{\partial t}\Big|_{\mathrm{adv}} = -\boldsymbol{\nabla}\cdot\boldsymbol{F}(\boldsymbol{U}). \tag{4.1}$$

The vector $\boldsymbol{U} = \varrho,\ \varrho\boldsymbol{V},\ E = (u_1, \ldots, u_5)$ represents in equation (4.1) the (density of) *conservative* quantities—mass, momentum, and energy, respectively, the vector $\boldsymbol{F}(\boldsymbol{U}) = \varrho\boldsymbol{V},\ \varrho\boldsymbol{V}\otimes\boldsymbol{V},\ E\boldsymbol{V}$ represents the flux of the same quantities (the distinction of total and partial derivatives is rather formal in this section, since both are solved numerically using the same finite difference method). The operator $\mathcal{L}$ represents all the mathematical functions (all the terms except the explicit time-derivatives) of the conservative quantities. The operator $\mathcal{L}$ can be split into parts, $\mathcal{L} = \mathcal{L}_1 + \mathcal{L}_2 + \ldots$, where each part represents a single term in the equations. We can thus sub-divide each time-step into m time-substeps which correspond to m RHS terms in each equation:

$$\begin{aligned} (u^1 - u^0)/\Delta t &= L_1(u^0), \\ (u^2 - u^1)/\Delta t &= L_2(u^1), \\ &\vdots \\ (u^m - u^{m-1})/\Delta t &= L_m(u^{m-1}), \end{aligned} \tag{4.2}$$

where L_i represent finite-difference approximations of $\mathcal{L}_i$, the superscripts refer to the time-substep and Δt is the interval of the time-step [11]. This scheme is of course an approximation of the exact solution, however, numerical experiments [21], [27] have shown that the multi-step procedure is more accurate than a single-step computation based on data calculated entirely in the previous time-step.

As already indicated in equation (4.1), the complete solution is within each time-step grouped into two global steps, the *source* and the *advection* (*transport*) steps. Within the *source* step, we solve the following finite-difference approximations of the

full set of hydrodynamic equations (introduced in standard cylindrical system) in the axisymmetric ($\partial/\partial\varphi = 0$) Lagrangian form [28]:

$$\left.\frac{\mathrm{d}\varrho}{\mathrm{d}t}\right|_{\text{source}} = 0, \tag{4.3}$$

$$\left.\frac{\mathrm{d}}{\mathrm{d}t}\Pi_R\right|_{\text{source}} = \varrho\frac{V_\varphi^2}{R} - \frac{\partial P}{\partial R} - \varrho\frac{GM_\star R}{(R^2+z^2)^{3/2}} - \frac{\partial Q}{\partial R}, \tag{4.4}$$

$$\left.\frac{\mathrm{d}J}{\mathrm{d}t}\right|_{\text{source}} = G_{R\varphi,\text{visc}}, \tag{4.5}$$

$$\left.\frac{\mathrm{d}}{\mathrm{d}t}\Pi_z\right|_{\text{source}} = -\frac{\partial P}{\partial z} - \varrho\frac{GM_\star z}{(R^2+z^2)^{3/2}} - \frac{\partial Q}{\partial z}, \tag{4.6}$$

$$\left.\frac{\mathrm{d}E}{\mathrm{d}t}\right|_{\text{source}} = -\frac{1}{R}\frac{\partial}{\partial R}[R(PV_R + q_R)] - \frac{\partial}{\partial z}(PV_z + q_z) + V_R G_{R\varphi,\text{visc}} + \Psi, \tag{4.7}$$

where Π_R and Π_z are the radial and the vertical momentum density components. Using the angular momentum J in equation (4.5) instead of azimuthal momentum component Π_φ, the solution experiences much greater stability [21] and the Coriolis force is automatically involved. The last term Ψ on the RHS of equation (4.7) represents the irreversible conversion of mechanical energy into heat (positive dissipation function),

$$\Psi = 2\eta E_{ij}E^{ij} + \Big(\zeta - \frac{2}{3}\eta\Big)\Big(\frac{\partial V_k}{\partial x_k}\Big)^2, \quad \text{where } E_{ij} = \frac{1}{2}\Big(\frac{\partial V_i}{\partial x_j} + \frac{\partial V_j}{\partial x_i}\Big) \tag{4.8}$$

is the Cauchy strain tensor and the term $E_{ij}E^{ij}$ denotes the inner product of two tensors E_{ij}, cf. [19]. In case of isothermal solution (see Section 2.2 for explanation) equation (4.7) drops out.

We employ in equations (4.4) and (4.6) the artificial viscosity Q in the explicit form [2], [21] that in the defined regions such as the compressive zones of shock waves acts as a bulk viscosity (we demonstrate here, e.g., the radial "piece" while the azimuthal "piece" is analogous)

$$Q_{R,i,j,k} = \varrho_{i,j,k}\Delta V_{R,i,j,k}[-C_1 a_{i,j,k} + C_2\min(\Delta V_{R,i,j,k}, 0)], \tag{4.9}$$

where $\Delta V_{R,i,j,k} = V_{R,i+1,j,k} - V_{R,i,j,k}$ is the forward difference of the radial velocity component, a is the sound speed and the lower indices i, j, k denote the ith, jth, and kth grid cell. The second term scaled by a constant $C_2 = 1.0$ is the quadratic artificial viscosity [2] used in compressive zones. The linear term with $C_1 = 0.5$ is used for damping numerical oscillations in stagnant regions of the flow [21].

We demonstrate the principle of the spatial derivative of the quantity u (located, e.g., on B-mesh) on the 1D example: we introduce left-side and right-side difference

quotients, $\Delta_-^{\mathrm{A}} = (u_i^{\mathrm{B}} - u_{i-1}^{\mathrm{B}})/(x_i^{\mathrm{B}} - x_{i-1}^{\mathrm{B}})$ and $\Delta_+^{\mathrm{A}} = (u_{i+1}^{\mathrm{B}} - u_i^{\mathrm{B}})/(x_{i+1}^{\mathrm{B}} - x_i^{\mathrm{B}})$, located at ith (or jth, kth in case of another coordinate directions) position of the grid. For the complete spatial differentiation we employ the (cell average) *van Leer* derivative [31], [32],

$$\mathrm{d}_{vL}^{\mathrm{B}} = \begin{cases} \langle \Delta_- \Delta_+ \rangle = \dfrac{2\Delta_-\Delta_+}{\Delta_- + \Delta_+}, & \text{if } \Delta_-\Delta_+ > 0, \\ 0, & \text{if } \Delta_-\Delta_+ < 0. \end{cases} \tag{4.10}$$

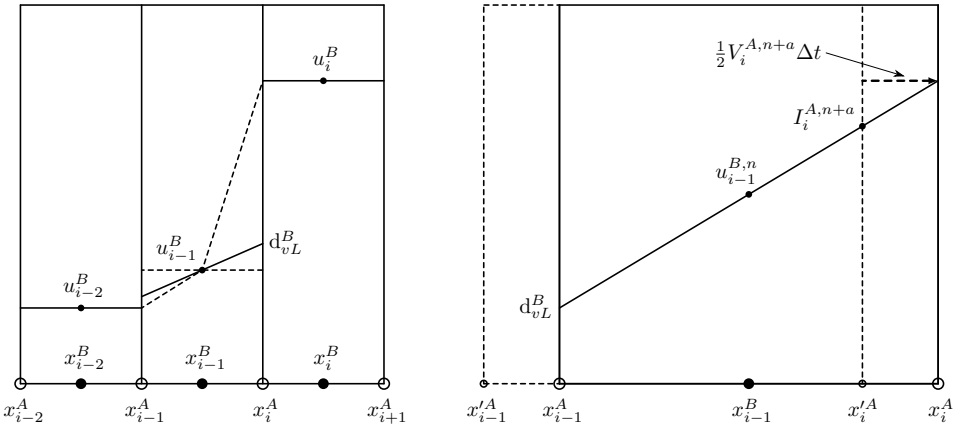

Figure 4. *Left panel*: scheme of the 1D van Leer derivative (equation (4.10)) whose slope (solid line denoted as d_{vL}^B) must fall on cell edges between the volume averages of the same quantity in two neighboring zones. Adapted from [31]. *Right panel*: 1D predictor step (equation (4.11)). A quantity u is advected on a cell edge in a half-time step $t + \Delta t/2$ along the van Leer derivative (solid line denoted as d_{vL}^B). The solid cell boundary depicts the fluid parcel advected in time $\Delta t/2$ while the dashed cell (with primed coordinates) is fixed in space. The position of the linear interpolant I is denoted by I_i^A. The corrector step (equation (4.12)) then advects the quantity in the center of the B-mesh cell in time $t + \Delta t$. Adapted from [11].

In the *advection* step (second equation in (4.1)) we use the two-step *predictor-corrector* algorithm for the calculation of time derivatives [7], [8], [22]. The intermediate (*predictor*) step is represented by the quantity I (*interpolant*). In case of the scalar quantity u (centered on the B-mesh) advected in the ith direction we have

$$I_{i,j,k}^{A,n+a} = u_{i-1,j,k}^{B,n} + \mathrm{d}_{vL}^B \Big(x_i^A - x_{i-1}^B - \frac{V_{i,j,k}^{A,n+a}\Delta t}{2} \Big), \tag{4.11}$$

where the superscript $n + a$ represents the partially updated nth time-step, x_A and x_B are the coordinates of the ith A-mesh and B-mesh point (see Fig. 4). The local advection velocity V^A is partially updated from the interpolant values I of the

momentum and density while it is updated once again at the end of the time-step. The subsequent *corrector* step is [6], [15], [16]

$$u^{B,n+1}_{i,j,k} = u^{B,n}_{i,j,k} - \frac{\Delta t}{\Omega^B_{i,j,k}}(I^{A,n+a}_{i+1,j,k} V^{A,n+a}_{i+1,j,k} S^A_{i+1,j,k} - I^{A,n+a}_{i,j,k} V^{A,n+a}_{i,j,k} S^A_{i,j,k}), \tag{4.12}$$

where $\Omega^B_{i,j,k}$ denotes the volume of the grid cell (control volume) centered on B-mesh at the grid point i, j, k and $S^A_{i,j,k}$ (control surface) denotes the area of the corresponding grid cell surface with normal vector oriented in the direction i. Equation (4.12) thus represents the numerical finite volume form of the *advection scheme* (equation (4.1)). The multidimensional advection is usually solved using the directional splitting which may involve a series of two or three one-dimensional partial updates, when each of them runs in different direction [28]. Each predictor step must lead to the exact location of the interpolant for the subsequent corrector step (we note that only the advected components of vector quantities are located at the A-mesh points while all the other components are treated as scalars). A detailed description of all parts of the calculation is very extensive and it is thus beyond the scope of this paper. For other numerical details as well as for the complete demonstration of the code structure including all routines and the MHD extension see [11].

4.2. Single-step (unsplit) finite volume scheme for calculation of extremely discontinuous flows with high Mach number. Following the principles of Roe's method [23], [29], we basically distinguish the vectors $\boldsymbol{W}$ of primitive and $\boldsymbol{U}$ of conservative (either for adiabatic or isothermal solution) hydrodynamic variables,

$$\boldsymbol{W} = \begin{pmatrix} \varrho \\ \boldsymbol{V} \\ P \end{pmatrix}, \quad \boldsymbol{U} = \begin{pmatrix} \varrho \\ \boldsymbol{\Pi} \\ E \end{pmatrix}. \tag{4.13}$$

The 3D Cartesian *advection scheme* (equation (4.1)) becomes the directionally split form,

$$\frac{\partial \boldsymbol{U}}{\partial t} + \frac{\partial \boldsymbol{\mathcal{F}}}{\partial x} + \frac{\partial \boldsymbol{\mathcal{G}}}{\partial y} + \frac{\partial \boldsymbol{\mathcal{H}}}{\partial z} = 0, \tag{4.14}$$

where $\boldsymbol{\mathcal{F}}$, $\boldsymbol{\mathcal{G}}$, and $\boldsymbol{\mathcal{H}}$ are the vectors of fluxes whose explicitly written components are

$$\boldsymbol{\mathcal{F}} = \begin{pmatrix} \varrho V_x \\ \varrho V_x^2 + P \\ \varrho V_x V_y \\ \varrho V_x V_z \\ (E+P)V_x \end{pmatrix}, \quad \boldsymbol{\mathcal{G}} = \begin{pmatrix} \varrho V_y \\ \varrho V_y V_x \\ \varrho V_y^2 + P \\ \varrho V_y V_z \\ (E+P)V_y \end{pmatrix}, \quad \boldsymbol{\mathcal{H}} = \begin{pmatrix} \varrho V_z \\ \varrho V_z V_x \\ \varrho V_z V_y \\ \varrho V_z^2 + P \\ (E+P)V_z \end{pmatrix}. \tag{4.15}$$

The linearized form of the conservation law can be written as

$$\frac{\partial \boldsymbol{U}}{\partial t} + \mathbf{A}_1^{\mathrm{C}}(\boldsymbol{U})\frac{\partial \boldsymbol{U}}{\partial x} + \mathbf{A}_2^{\mathrm{C}}(\boldsymbol{U})\frac{\partial \boldsymbol{U}}{\partial y} + \mathbf{A}_3^{\mathrm{C}}(\boldsymbol{U})\frac{\partial \boldsymbol{U}}{\partial z}, \tag{4.16}$$

$$\frac{\partial \boldsymbol{W}}{\partial t} + \mathbf{A}_1^{\mathrm{P}}(\boldsymbol{W})\frac{\partial \boldsymbol{W}}{\partial x} + \mathbf{A}_2^{\mathrm{P}}(\boldsymbol{W})\frac{\partial \boldsymbol{W}}{\partial y} + \mathbf{A}_3^{\mathrm{P}}(\boldsymbol{W})\frac{\partial \boldsymbol{W}}{\partial z}, \tag{4.17}$$

where the Jacobian matrices are $\mathbf{A}_1^{\mathrm{C}} = \partial\boldsymbol{\mathcal{F}}/\partial\boldsymbol{U}$, $\mathbf{A}_2^{\mathrm{C}} = \partial\boldsymbol{\mathcal{G}}/\partial\boldsymbol{U}$, $\mathbf{A}_3^{\mathrm{C}} = \partial\boldsymbol{\mathcal{H}}/\partial\boldsymbol{U}$, while $\mathbf{A}_1^{\mathrm{P}}(\boldsymbol{W}), \mathbf{A}_2^{\mathrm{P}}(\boldsymbol{W}), \mathbf{A}_3^{\mathrm{P}}(\boldsymbol{W})$ directly follow from the equations written in terms of $\boldsymbol{W}$. We introduce for simple illustration the Cartesian adiabatic hydrodynamic system expanded explicitly in the primitive variables $\boldsymbol{W} = (\varrho, V_x, V_y, V_z, P)$:

$$\frac{\partial \varrho}{\partial t} + V_x\frac{\partial \varrho}{\partial x} + \varrho\frac{\partial V_x}{\partial x} + V_y\frac{\partial \varrho}{\partial y} + \varrho\frac{\partial V_y}{\partial y} + V_z\frac{\partial \varrho}{\partial z} + \varrho\frac{\partial V_z}{\partial z} = 0, \tag{4.18}$$

$$\frac{\partial \boldsymbol{V}}{\partial t} + \Big(V_x\frac{\partial}{\partial x} + V_y\frac{\partial}{\partial y} + V_z\frac{\partial}{\partial z}\Big)\boldsymbol{V} + \frac{1}{\varrho}\Big(\hat{\mathbf{x}}\frac{\partial}{\partial x} + \hat{\mathbf{y}}\frac{\partial}{\partial y} + \hat{\mathbf{z}}\frac{\partial}{\partial z}\Big)P = 0, \tag{4.19}$$

$$\frac{\partial P}{\partial t} + \gamma P\Big(\frac{\partial V_x}{\partial x} + \frac{\partial V_y}{\partial y} + \frac{\partial V_z}{\partial z}\Big) + \Big(V_x\frac{\partial}{\partial x} + V_y\frac{\partial}{\partial y} + V_z\frac{\partial}{\partial z}\Big)P = 0, \tag{4.20}$$

while in the isothermal case equation (4.20) drops out.

The detailed demonstration of the complete Roe algorithm is highly beyond the scope of this paper, however, it is fully described, e.g., in [3], [23], [29]. The basic equation showing the computation of Roe fluxes is (in 1D simplification), see [27], [26],

$$\boldsymbol{F}_{i-1/2}^{\mathrm{Roe}} = \frac{1}{2}\Big[\boldsymbol{f}_{i-1/2}^{L} + \boldsymbol{f}_{i-1/2}^{R} + \sum_{\alpha}\mathbf{L}^{\alpha}\cdot(\boldsymbol{u}_{i-1/2}^{L} - \boldsymbol{u}_{i-1/2}^{R})|\lambda^{\alpha}|\mathbf{R}^{\alpha}\Big], \tag{4.21}$$

where $\boldsymbol{f}^L$, $\boldsymbol{f}^R$, $\boldsymbol{u}^L$, $\boldsymbol{u}^R$, are the volume-averaged fluxes ($\boldsymbol{f}$) and variables ($\boldsymbol{u}$) at the left and right cell interfaces at a half-timestep, λ^{α} are the eigenvalues of Roe matrices given in equations (4.25) and (4.33), and $\mathbf{L}^{\alpha}$, $\mathbf{R}^{\alpha}$, are the rows and columns of the left and right eigenmatrices (equations (4.26), (4.27), (4.30), (4.34), (4.38)) corresponding to λ^{α}. The time-updated values of $\boldsymbol{U}$ and $\boldsymbol{W}$ are calculated via the standard finite volume method [27]. In the next two paragraphs we demonstrate the explicit form of the Roe matrices in the "flaring disk" coordinates that can be used for modeling shocks in the disks, e.g., in case of disk-wind or disk-disk interactions or in case of binary or even multiple systems containing a compact component (neutron star).

4.3. Eigensystems of the flaring disk coordinates using Roe's method: adiabatic hydrodynamics. For adiabatic hydrodynamics in the *flaring disk coordinate frame* with the conservative variables $\boldsymbol{U} = (\varrho, \Pi_R, \Pi_\varphi, \Pi_\theta, E) = (u_1, \ldots, u_5)$

we write equation (4.14) in the vector form [29],

$$\frac{\partial \boldsymbol{U}}{\partial t} + \xi, \xi' \frac{\partial \boldsymbol{\mathcal{F}}}{\partial R} + \frac{1}{R}\frac{\partial \boldsymbol{\mathcal{G}}}{\partial \varphi} + \frac{\cos\theta}{R}\eta, \eta' \frac{\partial \boldsymbol{\mathcal{H}}}{\partial \theta} = \zeta, \zeta' \boldsymbol{\mathcal{S}}, \tag{4.22}$$

where $\boldsymbol{\mathcal{F}}$, $\boldsymbol{\mathcal{G}}$, $\boldsymbol{\mathcal{H}}$ are the vectors of fluxes in the R, φ, θ directions, respectively, and $\boldsymbol{\mathcal{S}}$ is the vector of geometric source terms that results from curvilinearity of the system. The factors $\xi = 1$, $\xi' = \sin\theta$ stand at particular R, θ components of the flux $\boldsymbol{\mathcal{F}}$, factors $\eta = 1$, $\eta' = \sin\theta$ stand at particular θ, R components of the flux $\boldsymbol{\mathcal{H}}$, factors $\zeta = 1$, $\zeta' = \sin\theta$ stand at particular R, θ components of the geometric source term $\boldsymbol{\mathcal{S}}$. The vectors $\boldsymbol{\mathcal{F}}$, $\boldsymbol{\mathcal{G}}$, $\boldsymbol{\mathcal{H}}$ written in the flaring disk coordinates are

$$\boldsymbol{\mathcal{F}},\ \boldsymbol{\mathcal{G}},\ \boldsymbol{\mathcal{H}} = \begin{pmatrix} u_{2-4},\ u_3,\ u_{4-2} \\ \dfrac{u_{2-4}u_2}{u_1} + \gamma_1\Big[u_5 - \dfrac{u_2^2+u_3^2+u_4^2}{2u_1}\Big],\ \dfrac{u_3u_2}{u_1},\ \dfrac{u_{4-2}u_2}{u_1} \\ \dfrac{u_{2-4}u_3}{u_1},\ \dfrac{u_3^2}{u_1} + \gamma_1\Big[u_5 - \dfrac{u_2^2+u_3^2+u_4^2}{2u_1}\Big],\ \dfrac{u_{4-2}u_3}{u_1} \\ \dfrac{u_{2-4}u_4}{u_1},\ \dfrac{u_3u_4}{u_1},\ \dfrac{u_{4-2}u_4}{u_1} + \gamma_1\Big[u_5 - \dfrac{u_2^2+u_3^2+u_4^2}{2u_1}\Big] \\ \Big[\gamma u_5 - \gamma_1\dfrac{u_2^2+u_3^2+u_4^2}{2u_1}\Big]\Big(\dfrac{u_{2-4}}{u_1},\ \dfrac{u_3}{u_1},\ \dfrac{u_{4-2}}{u_1}\Big) \end{pmatrix}, \tag{4.23}$$

where $u_{2-4} = u_2 - u_4$, $u_{4-2} = u_4 - u_2$, and $\gamma_1 = \gamma - 1$, demonstrating the swapping of components of momentum [26], [27]. The adiabatic conservative Jacobian matrices are $\mathbf{A}^{\mathrm{C}} = \partial(\boldsymbol{\mathcal{F}}, \boldsymbol{\mathcal{G}}, \boldsymbol{\mathcal{H}})/\partial \boldsymbol{U}$, where we hereafter denote $\mu = \cos\theta$, $V' = V_R - V_\theta \sin\theta$, and $H = (E+P)/\varrho$ is the enthalpy (noting that the factor $\sin\theta$ in the terms u_{2-4} and u_{4-2} is not differentiated), are

$$\mathbf{A}_1^{\mathrm{C}} = \begin{pmatrix} 0 & 1 & 0 & -\sin\theta & 0 \\ \gamma_1\dfrac{V^2}{2} - V_RV' & V' - \gamma_2 V_R & -\gamma_1 V_\varphi & V'' - \gamma V_\theta & \gamma_1 \\ -V_\varphi V' & V_\varphi & V' & -V_\varphi\sin\theta & 0 \\ -V_\theta V' & V_\theta & 0 & V' - V_\theta\sin\theta & 0 \\ \gamma_1\dfrac{V'V^2}{2} - V'H & H - \gamma_1 V_R V' & -\gamma_1 V_\varphi V' & -H\sin\theta - \gamma_1 V_\theta V' & \gamma V' \end{pmatrix},$$

$$\mathbf{A}_2^{\mathrm{C}} = \frac{1}{R}\begin{pmatrix} 0 & 0 & 1 & 0 & 0 \\ -V_\varphi V_R & V_\varphi & V_R & 0 & 0 \\ \gamma_1 - V_\varphi^2\dfrac{V^2}{2} & -\gamma_1 V_R & -\gamma_3 V_\varphi & -\gamma_1 V_\theta & \gamma_1 \\ -V_\varphi V_\theta & 0 & V_\theta & V_\varphi & 0 \\ \gamma_1\dfrac{V_\varphi V^2}{2} - V_\varphi H & -\gamma_1 V_R V_\varphi & H - \gamma_1 V_\varphi^2 & -\gamma_1 V_\varphi V_\theta & \gamma V_\varphi \end{pmatrix}, \tag{4.24}$$

$$\mathbf{A}_3^{\mathrm{C}} = \frac{\mu}{R}\begin{pmatrix} 0 & -\sin\theta & 0 & 1 & 0 \\ -V_R V'' & V'' - V_R\sin\theta & 0 & V_R & 0 \\ -V_\varphi V'' & -V_\varphi\sin\theta & V'' & V_\varphi & 0 \\ \gamma_1\dfrac{V^2}{2} - V_\theta V'' & V' - \gamma V_R & -\gamma_1 V_\varphi & V'' - \gamma_2 V_\theta & \gamma_1 \\ \gamma_1\dfrac{V''V^2}{2} - V''H & -H\sin\theta - \gamma_1 V_R V'' & -\gamma_1 V_\varphi V'' & H - \gamma_1 V_\theta V'' & \gamma V'' \end{pmatrix},$$

where $V'' = V_\theta - V_R\sin\theta$. The corresponding eigenvalues are

$$\begin{aligned} &\mathbf{A}_1^{\mathrm{C}}\colon\ \lambda_1^{\mathrm{C}} = (V' - a, V', V', V', V' + a), \\ &\mathbf{A}_2^{\mathrm{C}}\colon\ \lambda_2^{\mathrm{C}} = \frac{1}{R}(V_\varphi - a, V_\varphi, V_\varphi, V_\varphi, V_\varphi + a), \\ &\mathbf{A}_3^{\mathrm{C}}\colon\ \lambda_3^{\mathrm{C}} = \frac{\mu}{R}(V'' - a, V'', V'', V'', V'' + a), \end{aligned} \tag{4.25}$$

where a is the adiabatic speed of sound, $a^2 = \gamma P/\varrho$. The corresponding right eigenvectors of $\mathbf{A}_1^{\mathrm{C}}$ are the columns of the matrix

$$\mathbf{R}_1^{\mathrm{C}} = \begin{pmatrix} 1 & 0 & 0 & 1 & 1 \\ V_R - a & 0 & \sin\theta & V_R & V_R + a \\ V_\varphi & 1 & 0 & V_\varphi & V_\varphi \\ V_\theta & 0 & 1 & V_\theta & V_\theta \\ H - V'a & V_\varphi & \mu^2 V_\theta & \dfrac{V^2}{2} & H + V'a \end{pmatrix}, \tag{4.26}$$

while the matrices $\mathbf{R}_2^{\mathrm{C}}$ and $\mathbf{R}_3^{\mathrm{C}}$ are derived analogously. The corresponding left eigenvectors $\mathbf{L}_1^{\mathrm{C}}$ are the rows of the matrix

$$\mathbf{L}_1^{\mathrm{C}} = \begin{pmatrix} \dfrac{\gamma_1 V^2/2 + V'a}{2a^2} & -\dfrac{\gamma_1 V' + a}{2a^2} & -\dfrac{\gamma_1 V_\varphi}{2a^2} & -\dfrac{\gamma_1 V'' - a\sin\theta}{2a^2} & \dfrac{\gamma_1}{2a^2} \\ -V_\varphi & 0 & 1 & 0 & 0 \\ -V_\theta & 0 & 0 & 1 & 0 \\ 1 - \dfrac{\gamma_1 V^2}{2a^2} & \dfrac{\gamma_1 V'}{a^2} & \dfrac{\gamma_1 V_\varphi}{a^2} & \dfrac{\gamma_1 V''}{a^2} & -\dfrac{\gamma_1}{a^2} \\ \dfrac{\gamma_1 V^2/2 - V'a}{2a^2} & -\dfrac{\gamma_1 V' - a}{2a^2} & -\dfrac{\gamma_1 V_\varphi}{2a^2} & -\dfrac{\gamma_1 V'' + a\sin\theta}{2a^2} & \dfrac{\gamma_1}{2a^2} \end{pmatrix} \tag{4.27}$$

with analogous expressions for matrices $\mathbf{L}_2^{\mathrm{C}}$ and $\mathbf{L}_3^{\mathrm{C}}$.

For a comparison we introduce the same adiabatic system (4.18) in primitive variables $\boldsymbol{W} = (\varrho, V_R, V_\varphi, V_\theta, P) = (w_1, \dots, w_5)$ in the flaring disk coordinates:

$$
\begin{aligned}
&\frac{\partial \varrho}{\partial t} + \frac{1}{R}\Big[\frac{\partial (R\varrho V')}{\partial R} + \frac{\partial (\varrho V_\varphi)}{\partial \varphi}\Big] + \frac{\mu}{R}\Big(\varrho \delta V'' + V''\frac{\partial \varrho}{\partial \theta}\Big) = 0,\\
&\frac{\partial V_R}{\partial t} + V'\frac{\partial V_R}{\partial R} + \frac{V_\varphi}{R}\frac{\partial V_R}{\partial \varphi} + \frac{\mu}{R}V''\frac{\partial V_R}{\partial \theta} + \frac{1}{\varrho}\frac{\partial P}{\partial R} = 0,\\
&\frac{\partial V_\varphi}{\partial t} + V'\frac{\partial V_\varphi}{\partial R} + \frac{V_\varphi}{R}\frac{\partial V_\varphi}{\partial \varphi} + \frac{\mu}{R}V''\frac{\partial V_\varphi}{\partial \theta} + \frac{1}{\varrho R}\frac{\partial P}{\partial \varphi} = 0,\\
&\frac{\partial V_\theta}{\partial t} + V'\frac{\partial V_\theta}{\partial R} + \frac{V_\varphi}{R}\frac{\partial V_\theta}{\partial \varphi} + \frac{\mu}{R}\Big(V''\frac{\partial V_\theta}{\partial \theta} + \frac{1}{\varrho}\frac{\partial P}{\partial \theta}\Big) = 0,\\
&\frac{\partial P}{\partial t} + \frac{\gamma P}{R}\Big[\frac{\partial (RV')}{\partial R} + \frac{\partial V_\varphi}{\partial \varphi} + \mu \delta V''\Big] + (\gamma V)'\frac{\partial P}{\partial R} + \frac{V_\varphi}{R}\frac{\partial P}{\partial \varphi} + \frac{\mu(\gamma V)''}{R}\frac{\partial P}{\partial \theta} = 0,
\end{aligned}
\tag{4.28}
$$

where $(\gamma V)' = V_R - \gamma V_\theta \sin\theta$, $(\gamma V)'' = V_\theta - \gamma V_R \sin\theta$, and $\delta V'' = \partial_\theta V_\theta - \sin\theta \partial_\theta V_R$. In isothermal case (analogously to the Cartesian set (4.18)–(4.20)) the last equation (4.28) drops out. The adiabatic primitive matrices $\mathbf{A}_1^{\mathrm{P}}$, $\mathbf{A}_2^{\mathrm{P}}$, and $\mathbf{A}_3^{\mathrm{P}}$, become

$$
\mathbf{A}_1^{\mathrm{P}} = \begin{pmatrix} V' & \varrho & 0 & -\varrho\sin\theta & 0\\ 0 & V' & 0 & 0 & \dfrac{1}{\varrho}\\ 0 & 0 & V' & 0 & 0\\ 0 & 0 & 0 & V' & 0\\ 0 & \varrho a^2 & 0 & -\varrho a^2 \sin\theta & (\gamma V)' \end{pmatrix},\quad
\mathbf{A}_2^{\mathrm{P}} = \frac{1}{R}\begin{pmatrix} V_\varphi & 0 & \varrho & 0 & 0\\ 0 & V_\varphi & 0 & 0 & 0\\ 0 & 0 & V_\varphi & 0 & \dfrac{1}{\varrho}\\ 0 & 0 & 0 & V_\varphi & 0\\ 0 & 0 & \varrho a^2 & 0 & V_\varphi \end{pmatrix},
$$

$$
\mathbf{A}_3^{\mathrm{P}} = \frac{\mu}{R}\begin{pmatrix} V'' & -\varrho\sin\theta & 0 & \varrho & 0\\ 0 & V'' & 0 & 0 & 0\\ 0 & 0 & V'' & 0 & 0\\ 0 & 0 & 0 & V'' & \dfrac{1}{\varrho}\\ 0 & -\varrho a^2\sin\theta & 0 & \varrho a^2 & (\gamma V)'' \end{pmatrix}.
\tag{4.29}
$$

The corresponding eigenvalues λ_1^{P}, λ_2^{P}, λ_3^{P} of the matrices $\mathbf{A}_1^{\mathrm{P}}$, $\mathbf{A}_2^{\mathrm{P}}$, $\mathbf{A}_3^{\mathrm{P}}$ are identical with equation (4.25). The right and left eigenvectors, $\mathbf{R}_1^{\mathrm{P}}$ and $\mathbf{L}_1^{\mathrm{P}}$, are the respective columns and rows of the matrices

$$
\mathbf{R}_1^{\mathrm{P}} = \begin{pmatrix} 1 & 1 & 0 & 0 & 1\\ -\dfrac{a}{\varrho} & 0 & 0 & \sin\theta & \dfrac{a}{\varrho}\\ 0 & 0 & 1 & 0 & 0\\ 0 & 0 & 0 & 1 & 0\\ a^2 & 0 & 0 & 0 & a^2 \end{pmatrix},\quad
\mathbf{L}_1^{\mathrm{P}} = \begin{pmatrix} 0 & -\dfrac{\varrho}{2a} & 0 & \dfrac{\varrho\sin\theta}{2a} & \dfrac{1}{2a^2}\\ 1 & 0 & 0 & 0 & -\dfrac{1}{a^2}\\ 0 & 0 & 1 & 0 & 0\\ 0 & 0 & 0 & 1 & 0\\ 0 & \dfrac{\varrho}{2a} & 0 & -\dfrac{\varrho\sin\theta}{2a} & \dfrac{1}{2a^2} \end{pmatrix},
\tag{4.30}
$$

with analogously defined matrices for other directions. The vectors of adiabatic conservative and primitive geometrical source terms are $\boldsymbol{\mathcal{S}}^{\mathrm{C}} = -(\varrho V', \varrho \boldsymbol{V} V', \varrho V' H)^{\mathrm{T}}/R$, $\boldsymbol{\mathcal{S}}^{\mathrm{P}} = -(\varrho V', 0, \varrho a^2 V')^{\mathrm{T}}/R$.

4.4. Eigensystems of the flaring disk coordinates using Roe's method: isothermal hydrodynamics. In isothermal hydrodynamics in the *flaring disk coordinate frame* with the *conservative* variables $\boldsymbol{U} = (\varrho, \Pi_R, \Pi_\varphi, \Pi_\theta) = (u_1, \dots, u_4)$, the vectors of fluxes $\boldsymbol{\mathcal{F}}$, $\boldsymbol{\mathcal{G}}$, $\boldsymbol{\mathcal{H}}$ for R, φ, θ directions, respectively, have the form

$$\boldsymbol{\mathcal{F}}_{\mathrm{iso}}, \boldsymbol{\mathcal{G}}_{\mathrm{iso}}, \boldsymbol{\mathcal{H}}_{\mathrm{iso}} = \begin{pmatrix} u_{2-4}, u_3, u_{4-2} \\ \dfrac{u_{2-4}u_2}{u_1} + C^2 u_1, \dfrac{u_3 u_2}{u_1}, \dfrac{u_{4-2}u_2}{u_1} \\ \dfrac{u_{2-4}u_3}{u_1}, \dfrac{u_3^2}{u_1} + C^2 u_1, \dfrac{u_{4-2}u_3}{u_1} \\ \dfrac{u_{2-4}u_4}{u_1}, \dfrac{u_3 u_4}{u_1}, \dfrac{u_{4-2}u_4}{u_1} + C^2 u_1 \end{pmatrix}, \tag{4.31}$$

where C is the isothermal speed of sound. The isothermal conservative Jacobian matrices $\mathbf{A}^{\mathrm{C}}_{\mathrm{iso}} = \partial(\boldsymbol{\mathcal{F}}_{\mathrm{iso}}, \boldsymbol{\mathcal{G}}_{\mathrm{iso}}, \boldsymbol{\mathcal{H}}_{\mathrm{iso}})/\partial \boldsymbol{U}$ are

$$A^{\mathrm{C}}_{1,\mathrm{iso}} = \begin{pmatrix} 0 & 1 & 0 & -\sin\theta \\ -V_R V' + C^2 & V_R + V' & 0 & -V_R \sin\theta \\ -V_\varphi V' & V_\varphi & V' & -V_\varphi \sin\theta \\ -V_\theta V' & V_\theta & 0 & V' - V_\theta \sin\theta \end{pmatrix}, \tag{4.32}$$

$$A^{\mathrm{C}}_{2,\mathrm{iso}} = \frac{1}{R} \begin{pmatrix} 0 & 0 & 1 & 0 \\ -V_\varphi V_R & V_\varphi & V_R & 0 \\ -V_\varphi^2 + C^2 & 0 & 2V_\varphi & 0 \\ -V_\varphi V_\theta & 0 & V_\theta & V_\varphi \end{pmatrix},$$

$$A^{\mathrm{C}}_{3,\mathrm{iso}} = \frac{\mu}{R} \begin{pmatrix} 0 & -\sin\theta & 0 & 1 \\ -V_R V'' & V'' - V_R \sin\theta & 0 & V_R \\ -V_\varphi V'' & -V_\varphi \sin\theta & V'' & V_\varphi \\ -V_\theta V'' + C^2 & -V_\theta \sin\theta & 0 & V_\theta + V'' \end{pmatrix}.$$

The corresponding eigenvalues are

$$\begin{aligned} &\mathbf{A}^{\mathrm{C}}_{1,\mathrm{iso}}\colon\ \lambda^{\mathrm{C}}_{1,\mathrm{iso}} = (V' - C, V', V', V', V' + C), \\ &\mathbf{A}^{\mathrm{C}}_{2,\mathrm{iso}}\colon\ \lambda^{\mathrm{C}}_{2,\mathrm{iso}} = \frac{1}{R}(V_\varphi - C, V_\varphi, V_\varphi, V_\varphi, V_\varphi + C), \\ &\mathbf{A}^{\mathrm{C}}_{3,\mathrm{iso}}\colon\ \lambda^{\mathrm{C}}_{3,\mathrm{iso}} = \frac{\mu}{R}(V'' - C, V'', V'', V'', V'' + C). \end{aligned} \tag{4.33}$$

The right and left eigenvectors, $\mathbf{R}^{\mathrm{C}}_{1,\mathrm{iso}}$ and $\mathbf{L}^{\mathrm{C}}_{1,\mathrm{iso}}$, are the respective columns and rows of the matrices

$$\mathbf{R}^{\mathrm{C}}_{1,\mathrm{iso}} = \begin{pmatrix} 1 & 0 & 0 & 1 \\ V_R - C & 0 & \sin\theta & V_R + C \\ V_\varphi & 1 & 0 & V_\varphi \\ V_\theta & 0 & 1 & V_\theta \end{pmatrix}, \tag{4.34}$$

$$\mathbf{L}^{\mathrm{C}}_{1,\mathrm{iso}} = \begin{pmatrix} \dfrac{1+V'/C}{2} & -\dfrac{1}{2C} & 0 & \dfrac{\sin\theta}{2C} \\ -V_\varphi & 0 & 1 & 0 \\ -V_\theta & 0 & 0 & 1 \\ \dfrac{1-V'/C}{2} & \dfrac{1}{2C} & 0 & -\dfrac{\sin\theta}{2C} \end{pmatrix}, \tag{4.35}$$

in the radial direction (R) with analogously defined matrices for other directions. The isothermal hydrodynamic equations expressed in terms of primitive variables $\boldsymbol{W} = (\varrho, V_R, V_\varphi, V_\theta) = (w_1, \ldots, w_4)$ take the form

$$\begin{aligned} &\frac{\partial \varrho}{\partial t} + \varrho\Big(\frac{\partial V'}{\partial R} + \frac{1}{R}\frac{\partial V_\varphi}{\partial \varphi} + \frac{\mu}{R}\delta V''\Big) + V'\frac{\partial \varrho}{\partial R} + \frac{V_\varphi}{R}\frac{\partial \varrho}{\partial \varphi} + \frac{\mu}{R}V''\frac{\partial \varrho}{\partial \theta} = -\frac{\varrho V'}{R}, \\ &\frac{\partial V_R}{\partial t} + V'\frac{\partial V_R}{\partial R} + \frac{V_\varphi}{R}\frac{\partial V_R}{\partial \varphi} + \frac{\mu}{R}V''\frac{\partial V_R}{\partial \theta} + \frac{C^2}{\varrho}\frac{\partial \varrho}{\partial R} = 0, \\ &\frac{\partial V_\varphi}{\partial t} + V'\frac{\partial V_\varphi}{\partial R} + \frac{V_\varphi}{R}\frac{\partial V_\varphi}{\partial \varphi} + \frac{\mu}{R}V''\frac{\partial V_\varphi}{\partial \theta} + \frac{C^2}{\varrho R}\frac{\partial \varrho}{\partial \varphi} = 0, \\ &\frac{\partial V_\theta}{\partial t} + V'\frac{\partial V_\theta}{\partial R} + \frac{V_\varphi}{R}\frac{\partial V_\theta}{\partial \varphi} + \frac{\mu}{R}V''\frac{\partial V_\theta}{\partial \theta} + \frac{\mu}{R}\frac{C^2}{\varrho}\frac{\partial \varrho}{\partial \theta} = 0. \end{aligned} \tag{4.36}$$

The adiabatic primitive matrices $\mathbf{A}^{\mathrm{P}}_1$, $\mathbf{A}^{\mathrm{P}}_2$, and $\mathbf{A}^{\mathrm{P}}_3$ become

$$\mathbf{A}^{\mathrm{P}}_{1,\mathrm{iso}} = \begin{pmatrix} V' & \varrho & 0 & -\varrho\sin\theta \\ \dfrac{C^2}{\varrho} & V' & 0 & 0 \\ 0 & 0 & V' & 0 \\ 0 & 0 & 0 & V' \end{pmatrix}, \quad \mathbf{A}^{\mathrm{P}}_{2,\mathrm{iso}} = \frac{1}{R}\begin{pmatrix} V_\varphi & 0 & \varrho & 0 \\ 0 & V_\varphi & 0 & 0 \\ \dfrac{C^2}{\varrho} & 0 & V_\varphi & 0 \\ 0 & 0 & 0 & V_\varphi \end{pmatrix}, \tag{4.37}$$

$$\mathbf{A}^{\mathrm{P}}_{3,\mathrm{iso}} = \frac{\mu}{R}\begin{pmatrix} V'' & -\varrho\sin\theta & 0 & \varrho \\ 0 & V'' & 0 & 0 \\ 0 & 0 & V'' & 0 \\ \dfrac{C^2}{\varrho} & 0 & 0 & V'' \end{pmatrix}.$$

The corresponding eigenvalues $\lambda^{\mathrm{P}}_{1,\mathrm{iso}}$, $\lambda^{\mathrm{P}}_{2,\mathrm{iso}}$, $\lambda^{\mathrm{P}}_{3,\mathrm{iso}}$, of the matrices $\mathbf{A}^{\mathrm{P}}_{1,\mathrm{iso}}$, $\mathbf{A}^{\mathrm{P}}_{2,\mathrm{iso}}$, $\mathbf{A}^{\mathrm{P}}_{3,\mathrm{iso}}$, are identical with equation (4.33). The right and left eigenvectors, $\mathbf{R}^{\mathrm{P}}_{1,\mathrm{iso}}$ and

$\mathbf{L}^{\mathrm{P}}_{1,\mathrm{iso}}$, are the respective columns and rows of the matrices

$$\mathbf{R}^{\mathrm{P}}_{1,\mathrm{iso}} = \begin{pmatrix} 1 & 0 & 0 & 1 \\ -\dfrac{C}{\varrho} & \sin\theta & 0 & \dfrac{C}{\varrho} \\ 0 & 0 & 1 & 0 \\ 0 & 1 & 0 & 0 \end{pmatrix}, \quad \mathbf{L}^{\mathrm{P}}_{1,\mathrm{iso}} = \begin{pmatrix} \dfrac{1}{2} & -\dfrac{\varrho}{2C} & 0 & \dfrac{\varrho\sin\theta}{2C} \\ 0 & 0 & 1 & 0 \\ 0 & 0 & 0 & 1 \\ \dfrac{1}{2} & \dfrac{\varrho}{2C} & 0 & -\dfrac{\varrho\sin\theta}{2C} \end{pmatrix}, \tag{4.38}$$

with the other directions analogous. The vectors of isothermal conservative and primitive geometrical source terms are $\boldsymbol{\mathcal{S}}^{\mathrm{C}}_{\mathrm{iso}} = -(\varrho V', \varrho \boldsymbol{V} V')^{\mathrm{T}}/R$, $\boldsymbol{\mathcal{S}}^{\mathrm{P}}_{\mathrm{iso}} = -(\varrho V', 0)^{\mathrm{T}}/R$.

5. Results of time-dependent models

5.1. 2D models of the disks. We performed all the demonstrated models by employing both the numerical methods introduced in Sections 4.1 and 4.2 on a *flaring disk* grid, logarithmically scaled in the radial (R) direction, with the outer radius of the computational domain extending up to $500\,R_{\mathrm{eq}}$. The necessity of using such a relatively large domain results from the need of the model convergence by its passing through the so-called sonic point (where the radial outflowing velocity V_R equals the speed of sound a), which is usually located at a distance of several hundred radii of the star (an order of 10^{10} km). The results introduced in this section thus cover only illustrative fragments of the total computational domain, e.g. Fig. 5. The number of computational grid cells was 500 in the radial and 200 in the vertical direction, involving the 2D parallelization using the MPI procedure. The physical time of the convergence of the model was in this case of the order of 2 years (≈ 800 days) while the computational time was approximately 1 week (the maximum number of parallel processes used was 100).

We calculated the evolution of gas-dynamic density and temperature of the inner disk self-consistently, i.e., within each time-step of the full hydrodynamic process (including the calculation of viscous heat generation) we included the outcomes of calculation of the irradiative heating from the outer source (central star) from separate subroutines (which are not described in this paper). The variations of the density structure are thus affected by the variations of the temperature distribution within the heated gas, and vice versa, during the process of convergence of computation (all other models published so far use either the fixed hydrodynamic structure of the gas for calculation of thermal and radiative models, or they parameterize the temperature, calculating the time-dependent gas-dynamics). We input the initial state of the disk assuming Keplerian rotation ($V_\varphi \sim R^{-1/2}$), zero radial outflow ($V_R = 0$), and the vertically integrated density $\Sigma \sim R^{-2}$ [whose $\Sigma(R_{\mathrm{eq}})$

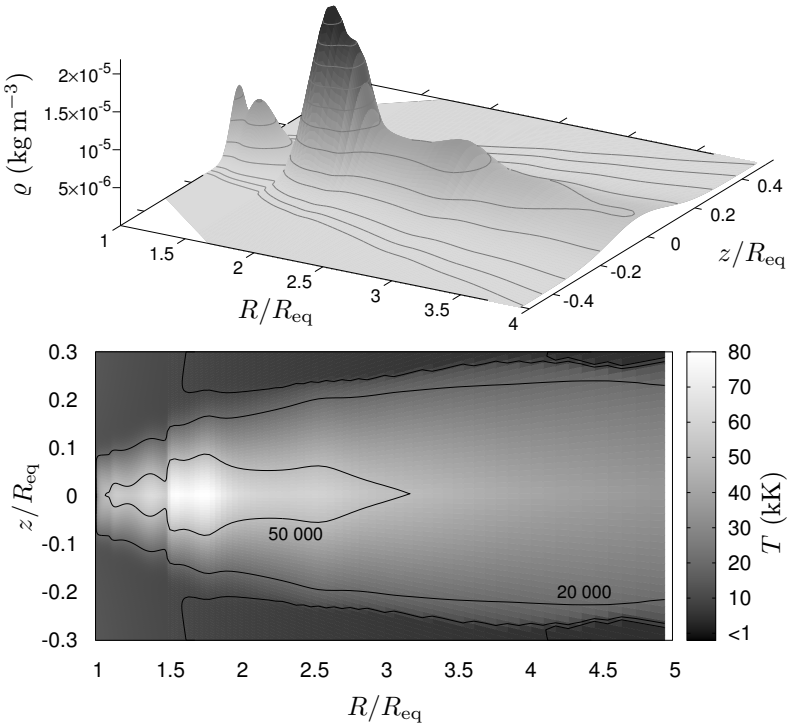

Figure 5. *Upper panel*: Self-consistent time-dependent calculations of the density structure of the inner part of a very dense circumstellar disk with mass-loss rate of approximately 10^{-6} solar masses per year [13] (where the parameter $R_{\rm eq}$ means the stellar equatorial radius). The contours mark the density levels (from low to high) 10^{-9}, 10^{-8}, 10^{-7}, 10^{-6}, 2.5×10^{-6}, 5×10^{-6} [kg m^{-3}], and so on, with the constant increment 2.5×10^{-6} kg m^{-3}. Physical time of the model convergence is approximately 2 years. *Lower panel*: Temperature structure of the same model as in the upper panel [13]. The region of significantly increased temperature near the disk midplane is generated by the viscous heating. The contours mark the temperature levels 10 000 K, 20 000 K, and 50 000 K. Thermal and radiative equilibria, electron and Kramers opacities, stellar equatorial and limb darkening, and radiative cooling are taken into account [13].

value follows the continuity equation], while we obtain the initial vertical density profile from equation (2.5). We parameterize the initial temperature distribution as $\partial T/\partial R \sim -pR^{-(p+1)}$, selecting the slope parameter p between 0 and 0.7, and $\partial T/\partial z = 0$. We use various boundary conditions for particular hydrodynamic quantities at the inner (stellar) boundary: the density ϱ and the angular momentum J are fixed (we assume there the non-varying Keplerian azimuthal velocity) while we set there the free boundary condition for the radial momentum flow Π_R (the zero vertical momentum flow Π_z results from the vertical hydrostatic equilibrium). We set the outer (right) boundary conditions as free for all the quantities. We assume

the lower and upper (left and right) boundary conditions in the vertical direction as outflow boundary conditions (or alternatively periodic, which does not significantly affect the computation) [11], [12].

5.2. Interactions of supernova expansion with circumstellar medium. We perform a model of the interaction of an expanding SN envelope with the ambient circumstellar media including a dense equatorial disk. The computation was performed on a Cartesian 2D grid with 300 grid cells in each direction, in a time interval up to 63 hours since the SN event. Prior to the envelope expansion we consider a strong shock (Sedov blast) wave in the SN progenitor interior that completely rearranges (homogenizes) its density structure [1]. The injected SN explosion energy is 10^{44} J. We consider the initial internal pressure as a homogeneous pressure of a photon gas (with $\gamma = 4/3$), $P_{\rm ini} = E/(3V) = E/(4\pi R_\star^3)$, i.e., of the order of 10^{11} Pa, while the initially isothermal pressure of the ambient medium may be of the order of 10^{-6} Pa and lower. The magnitude of the jump in pressure discontinuity thus grows up to 18 orders of magnitude (or even more) in the initial stage of interaction. The early phase of the SN envelope evolution can be basically described as adiabatic wave self-similar solution [4], [20], [24], where the time-dependent disk density structure is basically described in Section 2.3. Numerical solution is calculated using the method described in Section 4.2 [13], [27] that has proven itself in calculating such discontinuous, highly supersonic flows. We assume a stellar wind density of the spherically symmetric ambient medium $\varrho \propto r^{-2}$ and the disk structure is described in Sections 2.2 and 5.1. The models of density and expanding velocity are plotted in Fig. 6.

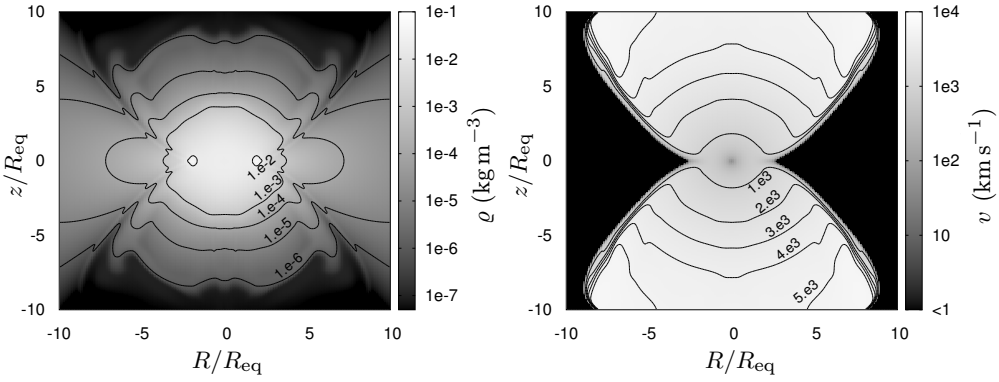

Figure 6. *Left panel*: Density structure from time-dependent calculation of adiabatic interaction between SN expansion ejecta and assymetric ambient medium, containing dense circumstellar disk along the horizontal midplane. Physical time of performed simulation: 63 hours since explosion. *Right panel*: Distribution of the expansion velocity in the same model. Adapted from [13].

6. Conclusions

We have developed two basic types of our own hydrodynamic (MHD) codes, employing two different numerical principles. Each of them fits to different nature of hydrodynamic processes. The operator-split finite volume Eulerian code (Section 4) fits to rather smooth hydrodynamic flows (where the pressure jump does not exceed some 2–3 orders of magnitude), while the unsplit finite volume scheme based on Roe's method (Section 4.2) was successfully used for calculations of processes with extremely large discontinuities and flows with high Mach number. Most of the astrophysical processes are successfully calculated on both types of the codes, which significantly increases the reliability of the results. Both the codes use the full Navier-Stokes viscosity to calculate realistic viscous and dissipative effects. We have written both the types of the codes in the basic orthogonal geometries, i.e., Cartesian, cylindrical, and spherical, and they have been properly tested for typical problems such as the Riemann-Sod shock tube, or the Rayleigh-Taylor instability, etc. We also introduce the unique "*flaring disk*" non-orthogonal coordinate system, which naturally fits to calculations of accretion or decretion astrophysical disks, into which we have also transformed both types of these numerical codes.

Comparison of the two approaches basically described in Sections 4.1 and 4.2, in terms of computational accuracy and speed, more or less corresponds to their determination. Our tests and practical results confirm the general assumption that the smooth hydrodynamics operator split approach is (up to 2 times) faster and gives more accurate results for the problems that do not involve too strong shocks and that comprise large spatial volumes. Its creation and its geometrical modifications as well as implementations of additional subroutines and various physical source terms is significantly easier than in case of the unsplit code. However, when the ratio L/a (where L and a are the typical length scale of a system and the characteristic speed of sound, respectively), which may roughly express the relaxation time, does not exceed 10^7–10^8 s (noting that in the disks $L/a \gtrsim 10^9$ s), the computational efficiency of the unsplit approach becomes comparable or even begins to dominate. In case of large discontinuities when the density or pressure jumps exceed 2–3 orders of magnitude, only the unsplit code is able to successfully calculate such a process, probably even for unlimited jumps in these characteristics (we have already tested maximum of some 40 orders of magnitude jump in pressure).

References

[1] *D. Arnett*: Supernovae and Nucleosynthesis: An Investigation of the History of Matter, from the Big Bang to the Present. Princeton Series in Astrophysics, Princeton University Press, 1996.

[2] *E. J. Caramana, M. J. Shashkov, P. P. Whalen*: Formulations of artificial viscosity for multi-dimensional shock wave computations. J. Comput. Phys. *144* (1998), 70–97. MR doi

[3] *P. Cargo, G. Gallice*: Roe matrices for ideal MHD and systematic construction of Roe matrices for systems of conservation laws. J. Comput. Phys. *136* (1997), 446–466. zbl MR doi

[4] *R. A. Chevalier*: Self-similar solutions for the interaction of stellar ejecta with an external medium. Astrophys. J. *258* (1982), 790–797. doi

[5] *R. A. Chevalier, N. Soker*: Asymmetric envelope expansion of supernova 1987A. Astrophys. J. *341* (1989), 867–882. doi

[6] *T. J. Chung*: Computational Fluid Dynamics. Cambridge University Press, Cambridge, 2002. zbl MR doi

[7] *C. Hirsch*: Numerical Computation of Internal and External Flows. Volume 1: Fundamentals of Numerical Discretization. Wiley Series in Numerical Methods in Engineering, Wiley-Interscience Publication, Chichester, 1988. zbl

[8] *C. Hirsch*: Numerical Computation of Internal and External Flows. Volume 2: Computational Methods for Inviscid and Viscous Flows. Wiley Series in Numerical Methods in Engineering, John Willey & Sons, Chichester, 1990. zbl

[9] *J. Krtička, P. Kurfürst, I. Krtičková*: Magnetorotational instability in decretion disks of critically rotating stars and the outer structure of Be and Be/X-ray disks. Astron. Astrophys. *573* (2015), A20, 7 pages. doi

[10] *J. Krtička, S. P. Owocki, G. Meynet*: Mass and angular momentum loss via decretion disks. Astron. Astrophys. *527* (2011), A84, 9 pages. doi

[11] *P. Kurfürst*: Models of Hot Star Decretion Disks. PhD Thesis, Masaryk University, Brno, 2015.

[12] *P. Kurfürst, A. Feldmeier, J. Krtička*: Time-dependent modeling of extended thin decretion disks of critically rotating stars. Astron. Astrophys. *569* (2014), A23. doi

[13] *P. Kurfürst, A. Feldmeier, J. Krtička*: Modeling sgB[e] circumstellar disks. The B[e] Phenomenon: Forty Years of Studies. Proc. Conf., Praha 2016, Astron. Soc. Pacific Conf. Ser. 508, Astronomical Society of the Pacific, San Francisco, 2017, pp. 17.

[14] *U. Lee, Y. Saio, H. Osaki*: Viscous excretion discs around Be stars. Mon. Not. R. Astron. Soc. *250* (1991), 432–437. doi

[15] *R. J. LeVeque*: Nonlinear conservation laws and finite volume methods. Computational Methods for Astrophysical Fluid Flow (O. Steiner et al., eds.). Saas-Fee Advanced Course 27, Lecture notes 1997, Swiss Society for Astrophysics and Astronomy, Springer, Berlin, 1998. zbl doi

[16] *R. J. LeVeque*: Finite Volume Methods for Hyperbolic Problems. Cambridge Texts in Applied Mathematics, Cambridge University Press, Cambridge, 2002. zbl MR doi

[17] *A. Maeder*: Physics, Formation and Evolution of Rotating Stars. Springer, Berlin, Heidelberg, 2009. doi

[18] *D. Mihalas*: Stellar Atmospheres. W. H. Freeman and Co., San Francisco, 1978.

[19] *D. Mihalas, B. W. Mihalas*: Foundations of Radiation Hydrodynamics. Oxford University Press, New York, 1984. zbl MR

[20] *D. K. Nadyozhin*: On the initial phase of interaction between expanding stellar envelopes and surrounding medium. Astrophys. Space Sci. *112* (1985), 225–249. zbl doi

[21] *M. L. Norman, K.-H. A. Winkler*: 2-D Eulerian hydrodynamics with fluid interfaces, self-gravity and rotation. Astrophysical Radiation Hydrodynamics. NATO Advanced Science Institutes (ASIC, volume 188), Springer, Dordrecht, 1986, pp. 187–221. doi

[22] *P. J. Roache*: Computational Fluid Dynamics. Hermosa Publishers, Albuquerque, 1976. zbl MR
[23] *P. L. Roe*: Approximate Riemann solvers, parameter vectors, and difference schemes. J. Comput. Phys. *135* (1997), 250–258. zbl MR doi
[24] *L. I. Sedov*: Similarity and Dimensional Methods in Mechanics. Nauka, Moskva, 1987. (In Russian.) zbl MR
[25] *N. I. Shakura, R. A. Sunyaev*: Black holes in binary systems: Observational appearance. Astron. Astrophys. *24* (1973), 337–355.
[26] *M. A. Skinner, E. C. Ostriker*: The Athena astrophysical magnetohydrodynamics code in cylindrical geometry. Astrophys. J. Supp. Ser. *188* (2010), 290–311. doi
[27] *J. M. Stone, T. A. Gardiner, P. Teuben, J. F. Hawley, J. B. Simon*: Athena: A new code for astrophysical MHD. Astrophys. J. Supp. Ser. *178* (2008), 137–177. doi
[28] *J. M. Stone, M. L. Norman*: ZEUS-2D: A radiation magnetohydrodynamics code for astrophysical flows in two space dimensions. I—The hydrodynamic algorithms and tests. Astrophys. J. Supp. Ser. *80* (1992), 753–790. doi
[29] *E. F. Toro*: Riemann Solvers and Numerical Methods for Fluid Dynamics: A Practical Introduction. Springer, Berlin, 2009. zbl MR doi
[30] *J. K. Truelove, C. F. McKee*: Evolution of nonradiative supernova remnants. Astrophys. J. Supp. Ser. *120* (1999), 299–326. doi
[31] *B. van Leer*: Towards the ultimate conservative difference scheme. IV: A new approach to numerical convection. J. Comput. Phys. *23* (1977), 276–299. zbl doi
[32] *B. van Leer*: Flux-vector splitting for the Euler equations. Int. Conf. Numerical Methods in Fluid Dynamics. Lecture Notes in Physics 170, Springer, Berlin, 1982, pp. 507–512. doi
[33] *Ya. B. Zel'dovich, Yu. P. Raizer*: Physics of Shock Waves and High-Temperature Hydrodynamic Phenomena. Academic Press, New York, 1967. zbl

Authors' address: *Petr Kurfürst*, *Jiří Krtička*, Department of Theoretical Physics and Astrophysics, Masaryk University, Kotlářská 2, 611 37 Brno, Czech Republic, e-mail: `petrk@physics.muni.cz`, `krticka@physics.muni.cz`.